

Synergistic Dissociation-and-Trapping Effect to Promote Li-Ion Conduction in Polymer Electrolytes via Oxygen Vacancies

Yongli Song, Luyi Yang, Jiawen Li, Mingzheng Zhang, Yaohui Wang, Shunning Li, Shiming Chen, Kai Yang, Kang Xu,* and Feng Pan*

Despite their promised safety and mechanical flexibility, solvent-free polymer electrolytes suffer from low Li-ion conductivities due to poor dissociation of conducting salts and low Li⁺-transference numbers due to Li⁺-trapping by ether-linkages. In this work, the authors found that oxygen vacancies carried by nanosized Al₂O₃ fillers preferentially promotes Li⁺-conduction in poly(ethylene oxide) (PEO). These vacancies and free electrons therein, whose concentration can be tuned, effectively break up the ion pairs by weakening the Coulombic attraction within them, while simultaneously interacting with the anions, thus preferentially constraining the movement of anions. This synergistic dissociation-and-trapping effect leads to the significant and selective improvement in Li-ion conductivity. Solid state batteries built on such PEO-based electrolytes exhibits superior performance at high current density. This discovery reveals a molecular-level rationale for the long-observed phenomenon that certain inorganic nano-fillers improve ion conduction in PEO, and provides a universal approach to tailor superior polymer-based electrolytes for the next generation solid-state batteries.

1. Introduction

Solid-state batteries (SSBs) is considered the ideal next-generation electrochemical energy storage system to replace the commercial lithium-ion batteries (LIBs) due to their better safety

Y. Song, L. Yang, J. Li, M. Zhang, S. Li, S. Chen, K. Yang, F. Pan School of Advanced Materials

Peking University Shenzhen Graduate School

Shenzhen 518055, China E-mail: panfeng@pkusz.edu.cn

Y. Wang

State Key Laboratory of Physical Chemistry of Solid Surfaces College of Chemistry and Chemical Engineering

Xiamen University Xiamen 361005, China

К Хп

Battery Science Branch Sensor and Electron Devices Directorate Power and Energy Division US Army Research Laboratory

Adelphi, MD 20783, USA E-mail: conrad.k.xu.civ@mail.mil

The ORCID identification number(s) for the author(s) of this article can be found under https://doi.org/10.1002/smll.202102039.

DOI: 10.1002/smll.202102039

and higher energy densities.[1-5] As a key component in SSBs, solid-state electrolytes (SSEs) could either be solvent-free solid polymer electrolytes (SPEs) or inorganic solid electrolytes (ISEs). SPEs promise advantages over ISEs such as more intimate interfacing with electrode materials, lightweight, low cost, high flexibility, and processability, however, with ion conductivities being generally inferior to ISEs.[6-8] Polymers with ether-linkages, exemplified by poly(ethylene oxide) (PEO), constitute the main structural skeleton for SPEs, while no other polymer structure has been found to dissolve lithium salt as effectively as these ether (EO) units.[9,10] However, these ether-linkage also brought intrinsic disadvantages to PEO-based SPEs, that is, low ionic conductivity, especially at room temperature (10^{-6} to 10^{-5} S cm⁻¹),^[7] as well as low Li+-transference number, because the EO units preferentially solvate Li+, as

evidenced by its high donor number for Li^{+,[11]} This interaction in fact forms a tight cage that confines Li⁺ while presenting a high energy barrier for its migration. The Li⁺-mobility thus completely depend on the segmental motion of these EO units in the polymer chains. Meanwhile, PEO is also a semi-crystalline material, whose crystalline phase is completely insulating to Li⁺-migration owing to the frozen segmental motions upon crystallization.^[12] Various inorganic fillers (e.g., Al₂O₃,^[13,14] TiO₂,^[15] CeO₂,^[16] SiO₂,^[17] Sm₂O₃,^[18] and ISEs^[19-21]) have been widely used to improve the ion transport in PEO-based SPEs, on the superficial belief that the presence of these foreign phases would disrupt PEO crystallinity.^[9,22] The mechanism of how these nano-fillers promote Li⁺-migration was never thoroughly investigated on the molecular level.

Despite the macroscopic similarity of PEO-based SPE to a solid, the local environment that a Li⁺ sees in PEO matrix is actually more liquid-like, where Li⁺ is surrounded by O-rich solvation sheaths as in non-aqueous electrolytes, and Li⁺-transport must be coupled to such solvation sheaths constructed by polymer segments via Li-O coordination. [23] It has been well known in ionic conductor that the solvent which can better shield the ionic coulombic field from each other and dissociate lithium salt better obtain higher ionic conductivity. [24,25] In addition, the Li⁺-transference number ($t_{\text{Li+}}$) is generally low (below 0.2) because of the preferential solvation of Li⁺ by

Scheme 1. Proposed mechanism for fillers to promote ion pair dissociation and to facilitate anion trapping.

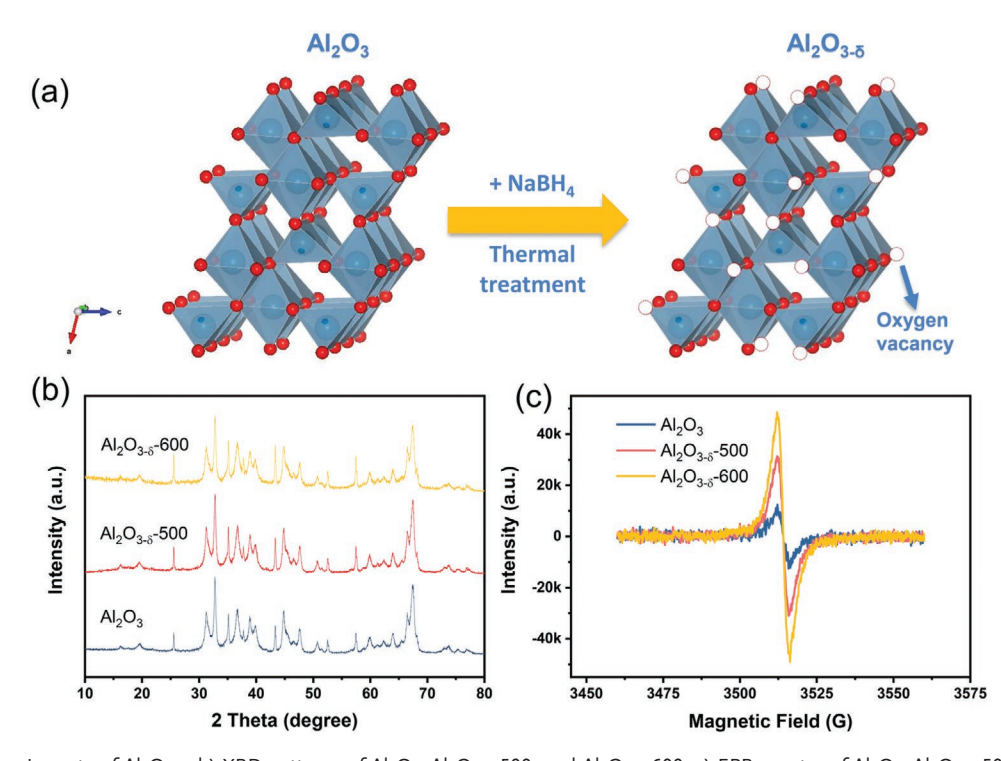
ether-linkages. Consequently, the "effective Li-ion conductivity" (which refers to the fraction of the ion conduction that is purely contributed by Li⁺-migration, and is defined as the product of overall ionic conductivity and $t_{\rm Li+}$ is often not benefited from the strategy of increasing overall ion conductivity only. In principle, an electrolyte with low transference number for the ions essential to cell reaction is undesirable, as the overall ion conductivity in this case only provides a deceptive impression of fast ion conduction but in fact cannot support the demand of mass-transport at high current densities.

In this work, by introducing nano-sized inorganic fillers (Al_2O_3) that carry oxygen vacancy at tunable concentrations, we revealed that the effective Li⁺ conductivity in PEO-based SPE is improved as result of two factors (**Scheme 1**): 1) free charges within polarizable fillers interact with ion pairs, generating localized induced dipole, which in turn weakens the coulombic attractions within the ion pairs and dissociates these ions; and 2) these fillers preferentially interact with anions, thus free Li⁺ to move. Through this simultaneous dissociate-and-trap mechanism, a higher concentration of free Li⁺ is available. Employing nano-sized Cu as a benchmarking reference, we further found

that this oxygen vacancy principle also applies to various fillers and lithium salts, thus providing us a universal guideline to tailor better SPEs for the next generation solid state batteries.

2. Result and Discussion

Oxygen vacancies were created in Al_2O_3 by mixing with NaBH₄ (**Figure 1**a), followed by thermal treatment at 500 and 600 °C. The obtained products are hereafter referred as $Al_2O_{3-\delta}$ 500 and $Al_2O_{3-\delta}$ 600, respectively. X-ray diffraction (XRD, Figure 1b) reveals that the nano-sized Al_2O_3 exhibits monoclinic C2/m space group, which barely changed during thermal treatment. The color change of Al_2O_3 (Figure S1, Supporting Information) clearly indicates that oxygen vacancies have been successfully introduced, while the darker $Al_2O_{3-\delta}$ 600 compared with lighter $Al_2O_{3-\delta}$ 500 suggests a higher oxygen vacancy concentration of the former as electrons trapped by oxygen vacancies are easily excited by light. [26–28] However, if the heating temperature further increases to 700 and 800 °C, Al_2O_3 undergoes a phase change into orthorhombic Pna21 space group (Figure S2,



 $\textbf{Figure 1.} \ \ \text{a) Synthesis route of } \ \text{Al}_2\text{O}_{3-\delta^{'}} \ \text{b) XRD patterns of } \ \text{Al}_2\text{O}_{3-\delta^{'}} 500, \ \text{and } \ \text{Al}_2\text{O}_{3-\delta^{'}} 600; \ \text{c) EPR spectra of } \ \text{Al}_2\text{O}_{3}, \ \text{Al}_2\text{O}_{3-\delta^{'}} 500, \ \text{and } \ \text{Al}_2\text{O}_{3-\delta^{'}} 600; \ \text{c)} \ \text{EPR spectra of } \ \text{Al}_2\text{O}_{3}, \ \text{Al}_2\text{O}_{3-\delta^{'}} 500, \ \text{and } \ \text{Al}_2\text{O}_{3-\delta^{'}} 600; \ \text{c)} \ \text{EPR spectra of } \ \text{Al}_2\text{O}_{3-\delta^{'}} 500, \ \text{and } \ \text{Al}_2\text{O}_{3-\delta^{'}} 600; \ \text{c)} \ \text{EPR spectra of } \ \text{Al}_2\text{O}_{3-\delta^{'}} 500, \ \text{and } \ \text{Al}_2\text{O}_{3-\delta^{'}} 600; \ \text{c)} \ \text{EPR spectra of } \ \text{Al}_2\text{O}_{3-\delta^{'}} 500, \ \text{and } \ \text{Al}_2\text{O}_{3-\delta^{'}} 600; \ \text{c)} \ \text{EPR spectra of } \ \text{Al}_2\text{O}_{3-\delta^{'}} 500, \ \text{and } \ \text{Al}_2\text{O}_{3-\delta^{'}} 600; \ \text{c)} \ \text{EPR spectra of } \ \text{Al}_2\text{O}_{3-\delta^{'}} 500, \ \text{and } \ \text{Al}_2\text{O}_{3-\delta^{'}} 600; \ \text{c)} \ \text{EPR spectra of } \ \text{Al}_2\text{O}_{3-\delta^{'}} 500, \ \text{and } \ \text{Al}_2\text{O}_{3-\delta^{'}} 600; \ \text{c)} \ \text{EPR spectra of } \ \text{EPR spectra of } \ \text{Al}_2\text{O}_{3-\delta^{'}} 500, \ \text{and } \ \text{Al}_2\text{O}_{3-\delta^{'}} 600; \ \text{c)} \ \text{EPR spectra of } \ \text{Al}_2\text{O}_{3-\delta^{'}} 500, \ \text{and } \ \text{Al}_2\text{O}_{3-\delta^{'}} 600; \ \text{c)} \ \text{EPR spectra of } \ \text{Al}_2\text{O}_{3-\delta^{'}} 500, \ \text{and } \ \text{Al}_2\text{O}_{3-\delta^{'}} 600; \ \text{c)} \ \text{EPR spectra of } \ \text{Al}_2\text{O}_{3-\delta^{'}} 500, \ \text{and } \ \text{Al}_2\text{O}_{3-\delta^{'}} 600; \ \text{c)} \ \text{EPR spectra of } \ \text{EPR spectra of } \ \text{Al}_2\text{O}_{3-\delta^{'}} 600; \ \text{c)} \ \text{Al}_2\text{O}_{3-\delta^{'}} 600; \ \text{c)} \ \text{EPR spectra of } \ \text{Al}_2\text{O}_{3-\delta^{'}} 600; \ \text{c)} \ \text{EPR spectra of } \$

16136829, 2021, 42, Downloaded from https:

/onlinelibrary.wiley.com/doi/10.1002/smll.202102039 by University Town Of Shenzhen, Wiley Online Library on [26/11/2025]. See the Terms and Conditions (https://onlinelibrary.wiley.com/terms/

conditions) on Wiley Online Library for rules of use; OA articles are governed by the applicable Creative Commons

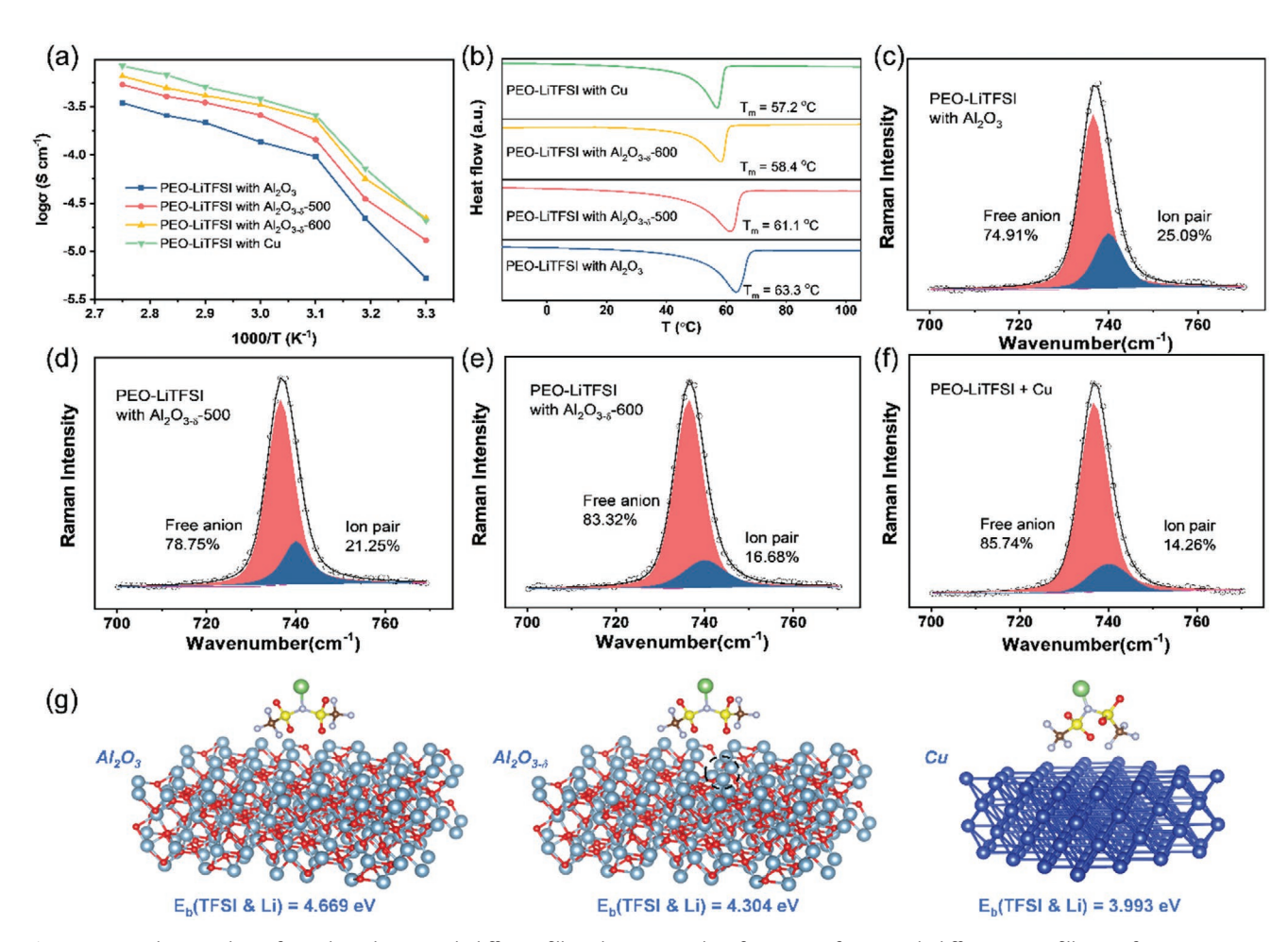


Figure 2. a) Arrhenius plots of PEO-based SPEs with different fillers; b) DSC results of patterns of SPES with different nano-fillers; c-f) Raman spectra of different SPEs and the corresponding peak resolving results; g) simulated results of binding energy between Li⁺ and TFSI⁻ at the surface of different nano-fillers.

Supporting Information), thus losing oxygen vacancy as powders exhibit no color change after sintering. Electron paramagnetic resonance (EPR) (Figure 1c) was employed to quantify the oxygen vacancy concentration. Since the EPR signals arise from the "free" electrons in oxygen vacancies, the increasing peak intensity from Al₂O₃ to Al₂O_{3-\delta}600 clearly reflects increasing oxygen vacancy concentrations in consistence with visual determination of the color change. It should be noted that the weak signal of Al₂O₃ can be attributed to the surface state of nanoparticles. In addition, the lowered binding energy for Al 2p in the X-ray photoelectron spectra (XPS, Figure S3, Supporting Information) also confirms the formation of oxygen vacancies.^[29] To understand the effect of free electrons, we introduced same amount of metallic Cu nanoparticles, which contain an infinite number of free electrons without oxygen vacancy, to PEO as a benchmarking nano-filler.

Lithium bis(trifluoromethane sulfonyl) imide (LiTFSI) was used as lithium salt in PEO for most experiments unless stated otherwise. In the Arrhenius plot (Figure 2a), the ionic conductivity of PEO-based SPEs at 60 °C are 1.36×10^{-4} , 2.59×10^{-4} , 3.31×10^{-4} , and 3.81×10^{-4} S cm⁻¹ for PEOs containing Al₂O₃, Al₂O₃₋₈500, Al₂O₃₋₈600, and Cu as nano-fillers, respectively. This result has confirmed our previous speculation in Scheme 1 that nano-fillers with higher free electron concentration (Al₂O_{3- δ}500 < Al₂O_{3- δ}600 < Cu) are more likely to dissociate ion pairs, leading to higher ionic conductivity. It should be noted that despite the electronic conducting nature of Cu particles, the high conductivity measured above should not have contribution from the electronic conductivity, because percolation Cu network is unavailable at such low Cu concentration. This is confirmed by the additional measurement of areal electronic conductivity of PEO-LiTFSI with various nano-fillers, which all ranged between 8.32×10^{-9} and 1.23×10^{-8} S cm⁻¹ (Figure S4, Supporting Information), indicating that the electronic conduction contributes very little to the overall conductivity. In the past literature reporting PEO containing nanofillers, the increase of ionic conductivity has always been attributed to the disruption of crystallinity and generation of more amorphous fraction. From the differential scanning calorimetry (DSC) results (Figure 2b), it is clearly shown that, in the presence of oxygen vacancies, the melting point of PEO-LiTFSI indeed decreases from 63.3 to 58.4 $^{\circ}\text{C}$, while the use of Cu further lowers the melting point to 57.2 °C, which agrees with the improved ionic conductivity.[30-32] The lowered glass-transition temperatures of PEO-LiTFSI with Cu and Al₂O₃₋₈600 (Figure S5, Supporting Information) also indicates poorer www.advancedsciencenews.com

crystallinity and higher segment mobility.[10] However, it should also be noted that, in the absence of Li salt, the melting point of PEO barely changes with the introduction of oxygen vacancies, which strongly implies that oxygen vacancies in Al₂O₃ fillers cast little influence on the crystallinity or segmental movement of PEO without Li salts (Figure S6, Supporting Information).

To resolve such seemingly conflicting phenomena and further identify the underlying mechanism, lithium salt association was investigated using Raman spectroscopy (Figure 2c-f), where the characteristic peak of TFSI⁻ indicates the degrees of ion dissociation. Deconvolution of this peak generates two peaks at wave number of 736.55 and 740.00 cm⁻¹, which should be assigned to free TFSI⁻ and Li⁺-TFSI⁻ ion pairs, respectively. Clearly the population of free TFSI- anions increases with the concentration of oxygen vacancies, indicating these vacancies promote the dissociation of LiTFSI. Computational simulation reveals that the binding energy between Li+ and TFSI- is reduced on the surface of Cu as well as Al₂O₃ with one adjacent oxygen vacancy compared to pristine Al₂O₃ (Figure 2g). In addition, the simulated charge density (Figure S7, Supporting Information) suggests that enrichment of charge density might occur around the oxygen vacancies. Therefore, it is reasonable to speculate that the Cu and Al₂O_{3-δ} shares a similar improving mechanism for ionic conductivity: the promotion of ion pair dissociation induced by the local dielectric environment that has been altered by the free electrons. In this case, the release of more Li+ is equivalent to increasing the Li salt concentration in the electrolyte, which requires additional polymer segments for coordination and inevitably disrupts the crystallinity of PEO. Therefore, the promoted mobility of PEO (i.e., lowered melting points and glass-transition temperatures) after the addition of oxygen modified Al2O3 or nano-Cu can be explained.

To further explore how Li+-migration in the PEO polymer matrix is affected, the Li⁺-transference number $(t_{\text{Li+}})$ for PEO-LiTFSI with different nano-fillers are measured (Figure 3a, see Figure S8, Supporting Information, for detailed data). Interestingly, Cu filler results in a $t_{1,i+}$ of 0.16, which is even lower than those of PEO with Al₂O₃ without the oxygen vacancies (0.18). In sharp contrast, the introduction of oxygen vacancies results in higher $t_{\text{Li+}}$ values -0.25 for Al₂O_{3- δ}500 and 0.27 for $Al_2O_{3-\delta}$ 600. Consequently, the effective Li⁺ conductivity can be calculated and compared in Arrhenius plots (Figure 3b), which shows that Al₂O_{3-\delta}600 far outperforms Cu with respect to the effective Li+ conductivity, despite the latter exhibiting higher overall ionic conductivity. The computation explains this discrepancy (Figure 3c) by demonstrating that oxygen vacancies preferentially bind to TFSI-anions, thus making them less mobile and leading to a higher $t_{[i]}$, [33,34] whereas fillers without oxygen vacancies such as Cu nanoparticles lack such interactions although they could improve the overall ionic conduction by dissociating Li-anion pairs.

To explore how the improved ion conductivity and Li⁺-transference number in these PEO SPEs impact actual cell operations, PEO with Al₂O₃₋₆600 was chosen as solid electrolyte to construct lithium metal batteries using lithium iron phosphate (LiFePO₄) as cathode, whose galvanostatic cycling is conducted at varied different current densities (Figure 4a). The cell with PEO + Al₂O_{3-\delta}600 electrolyte delivers higher capacities than PEO+Al₂O₃ as well as PEO+Cu at higher current densities, which is the direct result of higher effective Li-ion conductivity,

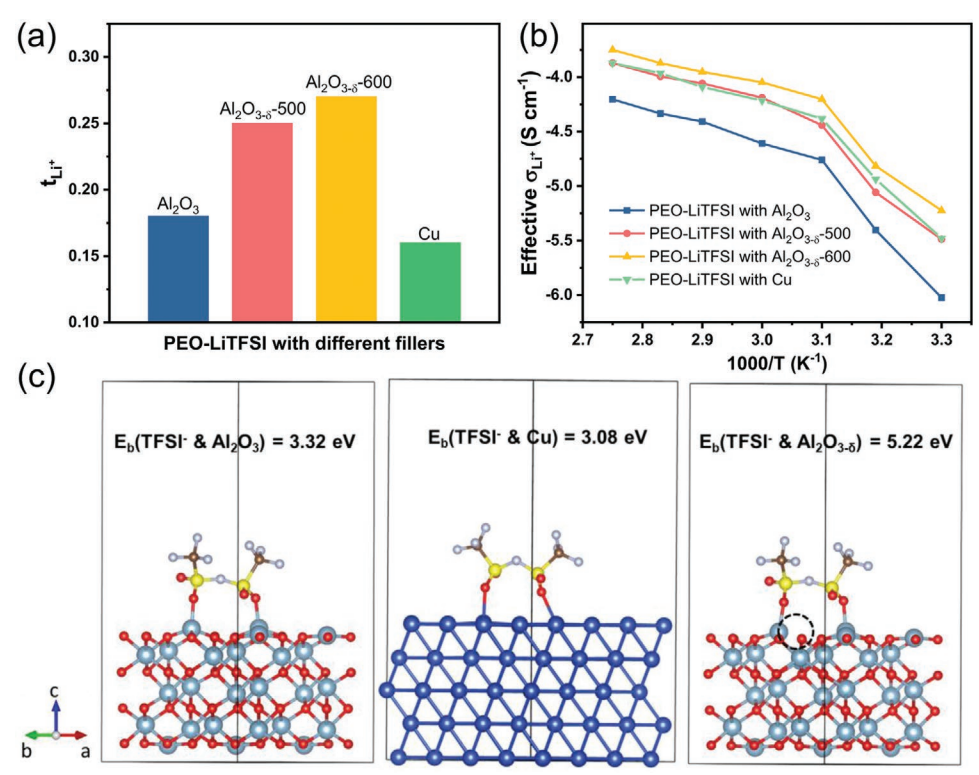


Figure 3. a) t_{1i+} and b) Arrhenius plots of effective Li⁺ conductivity for SPEs with different fillers; c) simulated bonding energy between TFSI⁻ anion and the surface of different nano-fillers.

16136829, 2021, 42, Downloaded from https://onlinelibrary.wiley.com/doi/10.1002/smll.202102039 by University Town Of Shenzhen, Wiley Online Library on [26/11/2025]. See the Terms

and Conditions (https://onlinelibrary.wiley.com/terms

conditions) on Wiley Online Library for rules of use; OA articles are governed by the applicable Creative Commons License

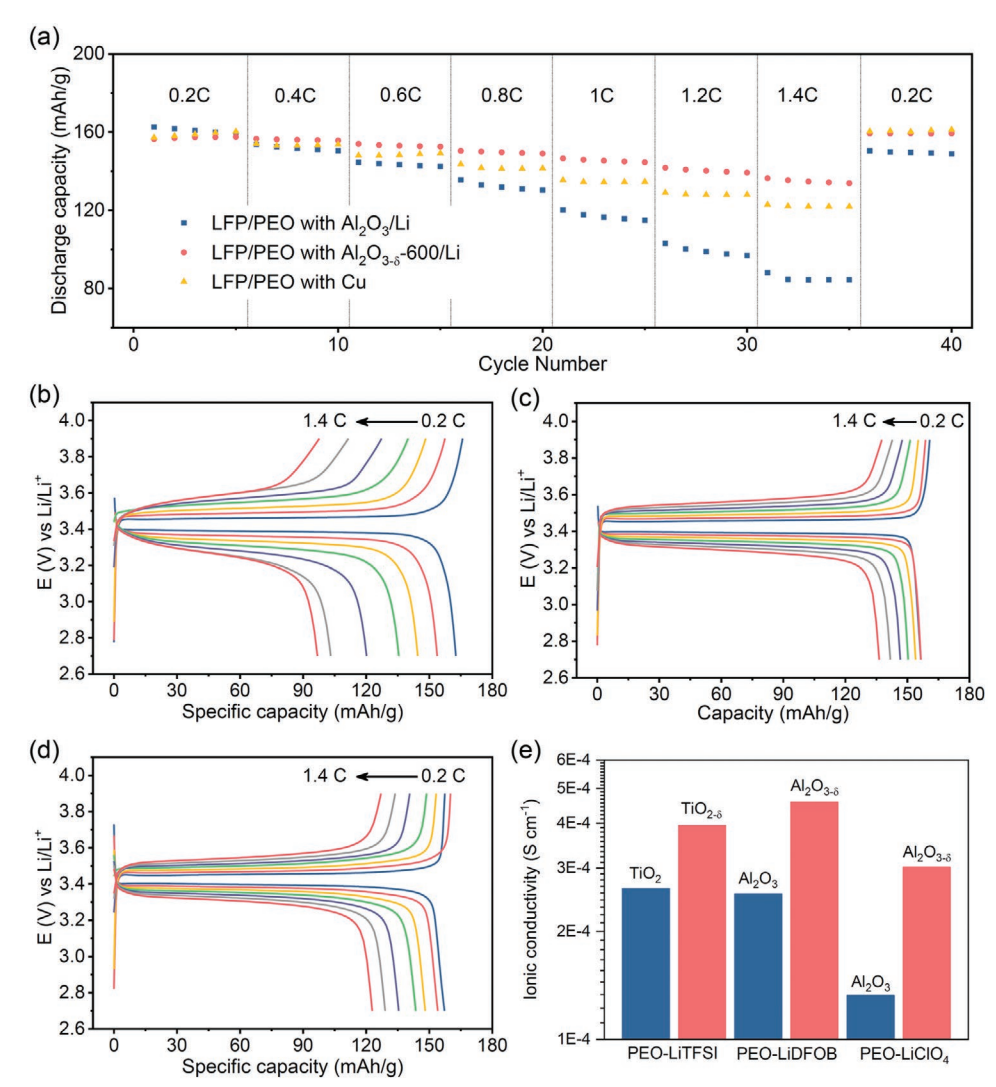


Figure 4. a) Galvanostatic cycling varied different current densities of solid-state full cells using different nano-fillers; potential profiles of b) PEO with Al_2O_3 , c) PEO with Al_2O_3 . ϵ 600, and d) PEO with Cu at different current densities. The areal loading of LFP at the positive electrode is \approx 2.3 mg cm⁻². All tests are carried out at 65 °C. e) Ionic conductivity of PEO-based SPEs with TiO₂ as fillers, LiClO₄ and LiDFOB as lithium salts at 70 °C.

indicating that the introduction of oxygen vacancies into Al₂O₃ could drastically improve ion transport to benefit the rate capability of cells. From the voltage profiles (Figure 4b-d), it can be clearly seen that the battery with PEO + $Al_2O_{3-\delta}$ 600 electrolyte not only showed much higher capacities, but also much reduced polarization between charging and discharging voltages, which agrees with the corresponding cyclic voltammograms (Figure S9, Supporting Information). In addition to the higher ionic conductivity, the lowered charge-transfer resistance as indicated by the semicircle at low frequency (Figure S10, Supporting Information), which arises from faster ion transport at electrode/electrolyte interfaces in both full cells and Li-Li symmetric cells. These results are also in accordance with the lowered polarization voltages in Li-Li symmetric cells (Figure S11, Supporting Information), further revealing the impact of nano-fillers on the rate performances.

To verify whether oxygen vacancy could be employed as a universal approach, we further tested the concept with other nano-fillers and lithium salts. Nano-sized ${\rm TiO_2}$ was treated at 250 °C to create oxygen vacancies, whose introduction into PEO displays rather similar improvement on ionic conductivity (Figure 4e), while LiTFSI was replaced by lithium perchlorate (LiClO₄) and lithium difluoro(oxalato)borate (LiDFOB), whose anions have completely different chemical structures. Nevertheless, Figure 4e reveals that the effect of oxygen vacancies on ionic conductivity is independent of the anions. Therefore, the correlation between oxygen vacancy and ion conduction established above can be widely applied to different systems.

3. Conclusion

In this study, we discovered that the oxygen vacancies brought by inorganic nanofillers serves as the key factor in promoting Li⁺-conduction. These oxygen vacancies weaken the Coulombic attraction between the ion pairs, thus dissociating them into

www.small-journal.com

free ions, and at the same time preferentially bind to the dissociated anions, thus promoting effective Li⁺-conduction. The fruition of these new SPEs enabled by oxygen vacancies is directly evidenced by the much-improved rate capability of the solid-state batteries thus constructed. Such dissociation-and-trapping mechanism provides a universal approach to tailor and design better polymer electrolytes for the next generation solid state batteries.

4. Experimental Section

Preparation of Fillers with Oxygen Vacancies: The oxygen vacancies in fillers were prepared by heating with NaBH₄ of equal mass in a vacuum tube furnace. For Al₂O₃ filler, 500 and 600 °C were used to create oxygen vacancies of different concentrations. For TiO₂ filler, oxygen vacancies were created by heating at 250 °C. The heating time was 10 h.

Preparation of SSE Film: The fillers, Li salts and PEO ($M_{\rm w}=4\times10^5$, Aldrich) were added to the anhydrous acetonitrile, and mechanically stirred for 12 h to form a homogeneous solution at a temperature of 70 °C. The solution was cast with a doctor blade on a polytetrafluoroethylene (PTFE) plate and dried in an argon-filled glove box at 80 °C for at least 12 h. For the PEO SSEs with Al₂O₃ based fillers, the weight ratio of PEO, Al₂O₃ based fillers and Li salt (LiTFSI, LiClO₄, LiFSI, and LiDFOB) was 600:25:16. For the PEO SSEs with TiO₂ based fillers, the weight ratio of PEO, fillers, and LiTFSI was 300:15:8. The weight ratio in PEO SSE with Cu power and LiTFSI was as same as PEO SSEs with Al₂O₃ based fillers.

Preparation of All-Solid-State LiFePO₄/SSE/Li Batteries: The ASSBs were assembled in 2032-type coin cells by contacting a Li metal anode, the as-prepared PEO SSE and a LiFePO₄ cathode. The cathode was composed of 70 wt% LiFePO4, 20 wt% carbon black, and 10 wt% PVDF binder. The cathode composite was added into NMP and then stirred for 12 h. Subsequently, the NMP solvent was removed at 80 °C in an oven, and then the electrode was punched with a diameter of 10 mm. The electrode sheets were stored in an argon-filled glove after drying for 12 h in vacuum oven at 100 °C. The batteries were sealed in an argon-filled glove box and then housed at 80 °C for 24 h to reduce the interfacial impedance between electrode and electrolyte. The areal loading of cathode was ≈2.3 mg cm⁻² and the thickness of Li anode was 500 μm.

Material Characterization: X-ray diffraction (XRD, Bruker D8 Advance powder X-ray diffractometer) was used to investigate the crystalline structure of Al_2O_3 based fillers and TiO_2 based fillers by scanning the angular range 10– 80° using CuKα radiation (λ = 1.5418 A). X-ray photoelectron spectroscopy (XPS, ESCALab220I-XL) and EPR (Bruker A300-10/12) were conducted to measure oxygen vacancies in fillers. Raman measurements were recorded using Xplora plus Raman spectrometer (HORIBA). A 50× microscope objective was used. The excitation wavelength was 785 nm. Raman spectrometer was calibrated using the characteristic Raman peak of silicon wafer 520.6 cm $^{-1}$.

Electrochemical Measurements: The ionic conductivities of SSE films were evaluated by the electrochemical impedance spectroscopy (EIS) with the frequency range of 0.1–10 6 Hz between 30 and 100 $^\circ$ C. The SSE films were sandwiched by two stainless steel disks. Ionic conductivity was calculated according to the equation:

$$\delta = \frac{L}{SR_b} \tag{1}$$

where L is the thickness of the electrolyte, R_b is the bulk resistance of the SSE, S is the area of the blocking stainless steel electrodes. The lithium transference number (t^+) for the SSE films was measured by chronoamperometry and AC impedance spectra using two lithium metal foils as the non-blocking electrodes. 10 mV was the potential applied across the cells, and electrochemical impedance spectroscopy (EIS) spectra of the cells before and after polarization were obtained from

0.1 to 10^6 Hz. The t^+ values for SSEs films were measured and calculated according to the equation:

$$t^{+} = \frac{I_{ss} \left(\Delta V - I_{0} R_{0} \right)}{I_{0} \left(\Delta V - I_{ss} R_{SS} \right)} \tag{2}$$

in which I_0 and $I_{\rm SS}$ are the initial and steady-state currents, ΔV is the polarization potential at 10 mV, and R_0 and $R_{\rm SS}$ are the initial and steady state resistance. The electrochemical tests were carried out using an electrochemical workstation (Solartron, 1400 cell test system). For cell performance with LiFePO₄ cathode and Li metal anode, the rate capability of SSBs was measured at 0.05, 0.1, 0.15, 0.2, 0.25, 0.3, 0.35, 0.4, 0.45, 0.5, 0.55, and 0.6mA cm⁻². All the batteries were tested between 2.7 and 3.9 V at 65 °C using an automatic galvanostatic charge discharge unit (Maccor, MC-16 Battery Test System).

Simulation Methods: The isomers of TFSI and TFSI-Li were optimized at B3LYP^[35,36]/6-311+G**^[37] level of theory using Gaussian09 package. Molecule orbitals were plotted via Multiwfn software^[38] and visual molecular dynamics (VMD).[39] Calculations for the adsorption of TFSI were performed using the plane wave DFT implemented in the Vienna ab initio simulation package (VASP)[40] with projector augmented wave (PAW) potentials.[41] The exchange-correlation interaction was treated within the generalized gradient approximation (GGA) of Perdew-Burke-Ernzerhof (PBE).[42] Valence electron configurations for the constituent elements were as follows: Li-2s¹, C-2s²2p², N-2s²2p³, O-2s²2p⁴, F-2s²2p⁵, and $Al-3s^23p^1$. The cut-off energy for the plane-wave expansion in structure optimization and energy calculation was set to 500 eV. Convergence was assumed when the total energy difference was below 1.0×10^{-5} eV per atom and the residual forces were below 0.02 eV Å⁻¹. The (001) surface of γAl_2O_3 was chosen to calculate the vacuum level, partial charge density, and adsorption energy. The surface structure was modeled by a supercell with a dimension of 9.61 Å \times 9.61 Å \times 23.3 Å which contained sixteen Al₂O₃ molecular units and 15 Å of the vacuum region. The Al₂O₃ slab and the adsorbed TFSI molecule were allowed to relax, and a (2 \times 2 \times 1) k-point grid determined by Monkhorst–Pack^[43] method was used to sample the Brillouin zone. The adsorption energy of TFSI on Cu (111) surface was also calculated. A (4 \times 4) supercell was constructed for the surface, above which a vacuum region of 15 Å was imposed. The calculation binding energy of Li to the TFSI which was on the different base is defined as the following:

$$\Delta E = E(\text{base/TFSI/Li}) - E(\text{Li}) - E(\text{base/TFSI})$$
(3)

Supporting Information

Supporting Information is available from the Wiley Online Library or from the author.

Acknowledgements

Y.S., L.Y., and J.L. contributed equally to this work. This work was financially supported by National Key R&D Program of China (2016YFB0700600).

Conflict of Interest

The authors declare no conflict of interest.

Data Availability Statement

Research data are not shared.

www.small-journal.com

Keywords

ion pair, ion transference number, ionic conductivity, oxygen vacancies

Received: April 15, 2021 Revised: June 29, 2021 Published online: September 15, 2021

- [1] J. Janek, W. G. Zeier, Nat. Energy 2016, 1, 16141.
- [2] R. Chen, Q. Li, X. Yu, L. Chen, H. Li, Chem. Rev. 2020, 120, 6820.
- [3] L. Xu, S. Tang, Y. Cheng, K. Wang, J. Liang, C. Liu, Y. Cao, *Joule* 2018, 2, 1991.
- [4] L. Yang, K. Yang, J. Zheng, K. Xu, K. Amine, F. Pan, Chem. Soc. Rev. 2020, 49, 4667.
- [5] S. Yang, R. He, Z. Zhang, Y. Cao, X. Gao, X. Liu, Matter 2020, 3, 27.
- [6] L. Fan, S. Wei, S. Li, Q. Li, Y. Lu, Adv. Energy Mater. 2018, 8, 170267.
- [7] D. Zhou, D. Shanmukaraj, A. Tkacheva, M. Armand, G. Wang, Chem 2019, 5, 2326.
- [8] Z. Wang, L. Yang, J. Liu, Y. Song, Q. Zhao, K. Yang, F. Pan, ACS Appl. Mater. Interfaces 2020, 12, 48677.
- [9] Z. Xue, X. Xie, J. Mater. Chem. A 2015, 3, 19218.
- [10] J. Mindemark, M. J. Lacey, T. Bowden, D. Brandell, *Prog. Polym. Sci.* 2018, 81, 114.
- [11] P. Johansson, Polymer 2001, 42, 4367.
- [12] S. Cheng, D. M. Smith, C. Y. Li, Macromolecules 2014, 47, 3978.
- [13] J. Zhou, P. S. Fedkiw, Solid State Ionics 2004, 166, 275.
- [14] R. Gao, R. Tan, L. Han, Y. Zhao, Z. Wang, L. Yang, F. Pan, J. Mater. Chem. A 2017, 5, 5273.
- [15] G. Hou, M. Zhang, L. Huang, W. Ruan, RSC Adv. 2016, 6, 83406.
- [16] A. Dey, S. Karan, J. Phys. Chem. Solids 2010, 71, 329.
- [17] L. Fan, C. Nan, S. Zhao, Solid State Ionics 2003, 164, 81.
- [18] P. P. Chu, M. J. Reddy, J. Power Sources 2003, 115, 288.
- [19] M. Liu, Z. Cheng, S. Ganapathy, C. Wang, L. A. Haverkate, M. Tułodziecki, S. Unnikrishnan, M. Wagemaker, ACS Energy Lett. 2019, 4, 2336.

- [20] J. Bi, D. Mu, B. Wu, J. Fu, H. Yang, G. Mu, L. Zhang, F. Wu, J. Mater. Chem. A 2020, 8, 706.
- [21] L. Yang, Z. Wang, Y. Feng, R. Tan, Y. Zuo, R. Gao, Y. Zhao, L. Han, Z. Wang, F. Pan, Adv. Energy Mater. 2017, 7, 1701437.
- [22] N. Boaretto, L. Meabe, M. Martinez-ibañez, M. Armand, H. Zhang, J. Electrochem. Soc. 2020, 167, 070524.
- [23] C. A. Angell, Electrochim. Acta 2017, 250, 368.
- [24] Y. Marcus, G. T. Hefter, Chem. Rev. 2006, 106, 4585.
- [25] M. Falco, C. Siman, C. Ferrara, J. R. Nair, G. Meligrana, F. Bella, I. Nicotera, P. Mustarelli, M. Winter, C. Gerbaldi, *Langmuir* 2019, 35, 8210
- [26] T. V. Perevalov, O. E. Tereshenko, V. A. Gritsenko, V. A. Pustovarov, A. P. Yelisseyev, C. Park, J. H. Han, C. Lee, J. Appl. Phys. 2010, 108, 013501.
- [27] D. Liu, S. J. Clark, J. Robertson, Appl. Phys. Lett. 2010, 96, 032905.
- [28] D. Liu, Y. Guo, L. Lin, J. Robertson, J. Appl. Phys. 2013, 114, 083704.
- [29] E. Ozensoy, J. Szanyi, C. H. F. Peden, J. Phys. Chem. B 2005, 109, 3431.
- [30] A. M. Rocco, R. P. Pereira, M. I. Felisberti, *Polymer* 2001, 42, 5199
- [31] M. J. Reddy, P. P. Chu, J. S. Kumar, U. V. Rao, J. Power Sources 2006, 161, 535.
- [32] M. J. Reddy, P. P. Chu, Solid State Ionics 2002, 149, 115.
- [33] H. Chen, D. Adekoya, L. Hencz, J. Ma, S. Chen, C. Yan, H. Zhao, G. Cui, S. Zhang, Adv. Energy Mater. 2020, 10, 2000049.
- [34] S. Batteries, N. Wu, P. Chien, Y. Qian, Y. Li, H. Xu, Angew. Chem., Int. Ed. Engl. 2020,59, 4131.
- [35] A. D. Becke, J. Chem. Phys. 1993, 98, 5648.
- [36] C. Lee, W. Yang, R. G. Parr, Phys. Rev. 1998, 37, 785.
- [37] M. J. Frisch, J. A. Pople, J. S. Binkley, J. Chem. Phys. 1984, 80, 3265.
- [38] T. Lu, F. Chen, J. Comput. Chem. 2012, 33, 580.
- [39] W. Humphrey, A. Dalke, K. Schulten, J. Mol. Graphics 1996, 14, 33.
- [40] G. Kresse, J. Furthmüller, Phys. Rev. B 1996, 54, 11169.
- [41] P. E. Blöchl, Phys. Rev. B 1994, 50, 17953.
- [42] J. P. Perdew, K. Burke, M. Ernzerhof, Phys. Rev. Lett. 1996, 77, 3865.
- [43] D. J. Chadi, Phys. Rev. B 1977, 16, 1746.